

**GT2011-450+\$**

## FILM-COOLED TRAILING EDGE MEASUREMENTS: 3D VELOCITY AND SCALAR FIELD

**Michael Benson**

U.S. Military Academy / Stanford University  
West Point, NY, USA

**Gregory Laskowski**

GE Global Research Center  
Niskayuna, NY, USA

**Chris Elkins**

Stanford University  
Stanford, CA, USA

**John K. Eaton**

Stanford University  
Stanford, CA, USA

### ABSTRACT

*Aircraft turbine blade trailing edges commonly are cooled by blowing air through pressure-side cutback slots. The surface effectiveness is governed by the rate of mixing of the coolant with the mainstream, which is typically much faster than predicted by CFD models. 3D velocity and coolant concentration fields were measured in and around a cutback slot using a simple uncambered airfoil with a realistic trailing edge cooling geometry at a Reynolds number of 110,000 based on airfoil chord length, which is lower than practical engines but still in the turbulent regime. The results were obtained using magnetic resonance imaging (MRI) techniques in a water flow apparatus. Magnetic resonance concentration (MRC) scans measured the concentration distribution with a spatial resolution of  $0.5 \text{ mm}^3$  (compared to a slot height of 5 mm) and an uncertainty near 5%. Magnetic resonance velocimetry (MRV) was used to acquire 3D, three-component mean velocity measurements with a resolution of  $1.0 \text{ mm}^3$ . Coupled concentration and velocity measurements were used to identify flow structures contributing to the rapid mixing, including longitudinal vortices and separation bubbles. Velocity measurements at several locations were compared with an unsteady RANS model. Concentration measurements extrapolated to the surface provided film cooling effectiveness and showed that the longitudinal vortices decreased effectiveness near the lands and reduced the average film cooling effectiveness.*

### INTRODUCTION

Gas turbine blades require specialized cooling schemes because turbine inlet temperatures exceed the material melting point. In order to minimize aerodynamic losses the trailing edge

should be kept as thin as possible. Cooling the trailing edge of a blade is especially critical and difficult because the blade thickness becomes too thin for internal cooling passages. In the trailing edge region, cutback configurations are commonly used where slots are cut into the pressure surface and separated by lands for structural support. Ideally, accurate models would allow for modifications to optimize the design and minimize the coolant flow over these important regions. Current models, even those that use unsteady conditions as in Holloway et al [1], Martini [2], and Joo and Durbin [3], continue to be challenged to accurately model the surface cooling effectiveness.

There have been significant efforts to experimentally study both the heat transfer coefficient and the adiabatic film cooling effectiveness at the surface of the cutback sections of the turbine blades [4-11]. While varied in measurement techniques and their similarity to engine conditions, each of the previous trailing edge studies focused on surface properties at the breakout surface or on the lands that separate the slots.

Developments using magnetic resonance imaging (MRI) techniques offer a new way to study the flow associated with trailing edges [12]. Advantages include rapid experimental results with reasonable uncertainties, the ability to use non-magnetic rapidly manufacturable stereolithography models for complex geometries, and no requirements for optical access. Limitations include matching realistic engine conditions.

The objective of the present work was to experimentally characterize the interaction between the coolant and mainstream fluids for a realistic three-dimensional (3D) trailing edge breakout geometry to gain insight into the 3D structures that contribute to the rapid mixing. Medical MRI scanners were

used to obtain both the 3D velocity and concentration fields. While the adiabatic film cooling surface effectiveness is discussed, the surrounding scalar field and contributing velocity field are also reported.

**TEST APPARATUS**

Complete details of the setup with coordinates are available in [13]. The critical sections of the apparatus are described briefly here. The geometry of the rectangular test section is shown in Figure 1.

The upstream portion is flow conditioning. The first three sections are diffusers with multiple grids to expand the flow from a 50 mm dia. inlet tube to a square cross-section 152 mm x 152 mm without separation. The fourth is a contraction that smoothly reduces the outlet of diffuser 3 to provide uniform flow to the 152 mm x 76 mm channel inlet. Contractions in the test section sidewalls surrounding the blade model airfoil reproduce the favorable pressure gradient and thin boundary layers common to turbine blades.

The flow model has a NACA-0012 airfoil as its basic shape with the final 5.7% of the chord blunted making it 283 mm long. Three cutback slots are spaced spanwise with the breakout surface covering the final 42.1 mm of the trailing edge. The slots are wider than their height in a direction normal to the breakout surface. The breakout surface is at an angle of 3.6° from the airfoil center plane. Cooling flow is fed through the top of the channel into a triangular shaped manifold, which smoothly transitions to a rectangular channel that feeds the cooling slots. Figure 2 shows side and top views of the airfoil.

The streamwise coordinate (x) begins at the airfoil leading edge, with streamwise dimensions normalized by slot height, h. The slot exit at 240.7mm is identified as  $x_s$ . The channel centerplane provides the origin for wall normal (y) and spanwise (z) coordinates, as shown in Figure 3, which also emphasizes the key features of the trailing edge. Note that the y-coordinate origin does not correspond to the surface of the sloped breakout. The mainstream and cooling fluids are metered with calibrated paddlewheel flow meters with a maximum uncertainty of 1.6%.

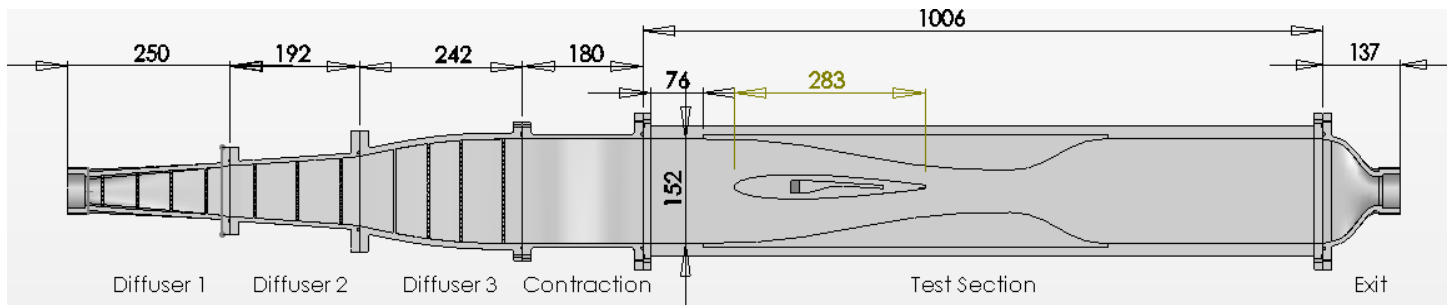


**Figure 1 - Cross-sectional top view of flow apparatus, with flow from left to right. Dimensions in mm**

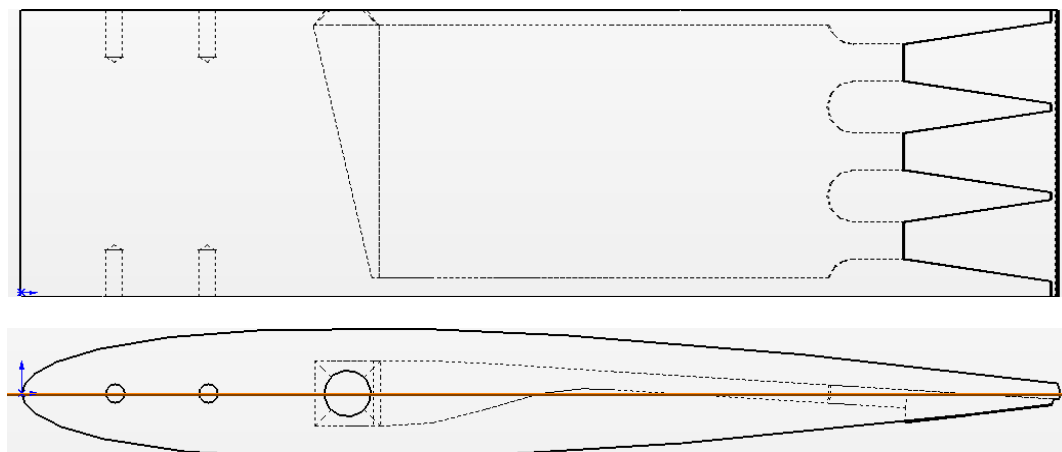


**Figure 2 - Side and top view of airfoil. Flow is left to right, with the y coordinate axis highlighted**

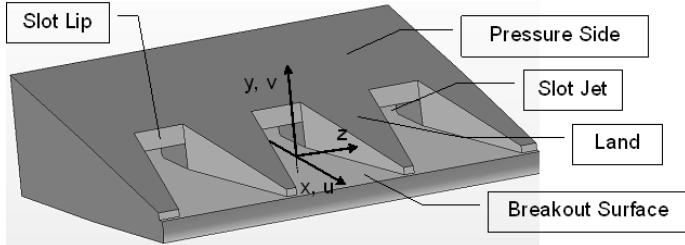


**Figure 3 - Key features of the trailing edge region**

**MAGNETIC RESONANCE IMAGING DETAILS**

The MRI system and procedure is essentially the same as that described in [14]. A 1.5 Tesla GE Signet magnet (model Signa HDX) is utilized with a standard head-imaging coil capable of transmitting and receiving radio frequency pulses. For the concentration measurements (MRC), the sequence used by the scanner is the same 3D Fast SPGR sequence described in [14]. The two mixing fluids were water and a solution of water and copper sulfate pentahydrate, with the water de-aerated prior to usage. The copper sulfate solution was 0.015 mol/liter, with a density difference of less than 0.8% from the plain water. The copper sulfate acts as a scalar contaminant and registers with an excellent signal to noise ratio for a T1-weighted magnitude scan. The signal magnitude from the copper sulfate solution scales linearly with the relative concentration.

The key scanning parameters utilized in the experiment were a 55° flip angle, an 11.5 ms repetition time (TR), a minimum echo time (TE), a bandwidth of 31.25 kHz, and a field of view of 25.6 cm. Frequency, phase, and slice encoding were done in the x, y, and z directions, respectively. The phase encoded field of view had a width of 9.2 cm.

Each MRC scan was 119 seconds in duration. Total scans for each scan type are listed in Table 1. Resolution for the concentration scans was 0.5 mm<sup>3</sup>, with 0.5 mm resolution in the y coordinate and 1 mm resolution in x and z. Concentration scans yielded intensity matrices within the flow that were 256 x 61 x 92 in the x, y, and z directions, respectively. In all, there were 1.44 million elements. Four scan types are needed for MRC scans: Reference, Background, Standard, and Inverted, and each scan is completed at the same flow rates for mainstream and coolant lines. Reference scans use copper sulfate solution as both the mainstream and coolant fluids, establishing the point by point 100% concentration signal for use in Equations 1-4. Background scans use plain water and are subtracted from the other three scan types. Standard runs have copper sulfate solution as the coolant fluid, and water as the mainstream. Inverted runs switch these two fluids. The equations for the concentration calculations are outlined in Equations 1-4. S indicates Standard magnitude, I is Inverted, B is Background, R is Reference, SF is a scale factor, and C is Concentration. The scale factor in Equation 1 is a single correction applied to the entire data set. Due to the length of the experiment, the MRI signal drifts 1-2%. This necessitates the SF which scales the reference case to match the sum of the

signal across all y and z elements from inverted and standard scans for each streamwise position, as outlined in [13, 14].

$$SF(x) = \frac{(S(x, y, z) - B(x, y, z)) + (I(x, y, z) - B(x, y, z))}{R(x, y, z) - B(x, y, z)} \quad (1)$$

$$R'(x, y, z) = SF(x) \times R(x, y, z) \quad (2)$$

$$C(x, y, z) = \frac{S(x, y, z) - B(x, y, z)}{R'(x, y, z) - B(x, y, z)} \quad (3)$$

$$C(x, y, z) = 1 - \frac{I(x, y, z) - B(x, y, z)}{R'(x, y, z) - B(x, y, z)} \quad (4)$$

Magnetic Resonance Velocimetry (MRV) scans were conducted as described in [15] immediately following the last concentration scan. Resolution was changed to 1 mm in the wall normal direction yielding 1.0 mm<sup>3</sup> resolution, in order to maintain a high signal to noise ratio and minimize uncertainty. Velocity encoding was to 90 cm/s in the streamwise, 50 cm/s in the spanwise, and 50 cm/s in the wall normal directions. In post-processing, the data were interpolated to match the concentration data field. Each MRV scan took 301 seconds. A flow-off scan preceded and followed each set of three flow-on scans. Uncertainty in the MRV measurements is 6.9% based on data agreement with the flowmeters as described in [15].

The apparatus was set up in the MRI scanner and then all the MRC/MRV scans, including all of the runs listed in Table 1, were completed in a single 18-hour session. Flowmeters were continuously monitored through all scans to ensure steady conditions were maintained.

Reference	Background	Standard	Inverted	Flow On	Flow Off
30	21	21	21	12	3

**Table 1 – Total number of scans conducted by run type**

**COMPUTATIONAL DETAILS**

A CFD model of the water channel was built to provide additional insight into the dynamics associated with trailing edge cooling. The computational domain consisted of the airfoil and internal flow path that supplied the slot. The middle slot was simulated and translationally periodic boundary conditions were utilized for computational efficiency. The tetrahedral mesh shown in Figure 4 had near wall inflation layers and the solution was verified as mesh independent. Near wall gridding ensured adequate resolution for wall integration simulations such that y<sup>+</sup> < 1.0 for all airfoil wall surfaces. Additional resolution was specified in the slot and wake region.

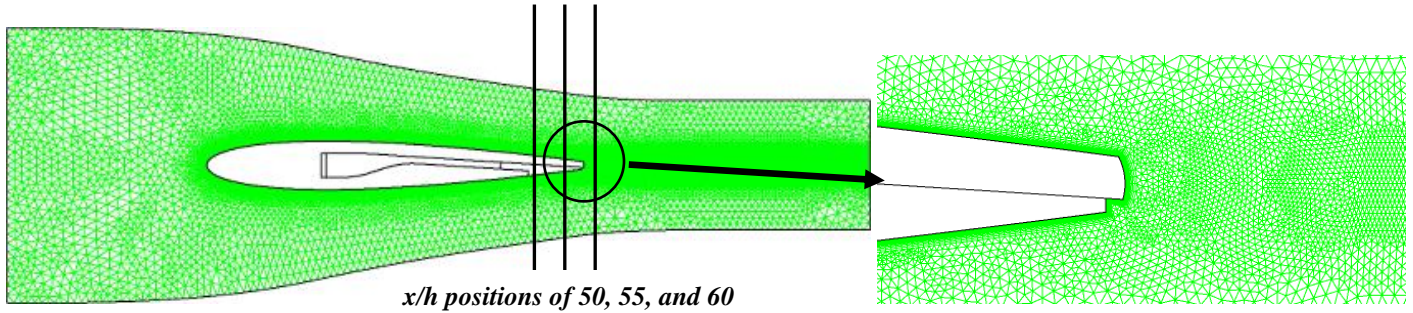


Figure 4 – CFD mesh for airfoil and channel simulation

Approximately 50 isotropic control volumes spanned the wake as can be seen in the expanded region shown in Figure 4. The Wilcox  $k-\omega$  turbulence model was selected for the simulations. The inlet mass flow measured in the experiment was specified for the primary flow as was the inlet mass flow for the secondary flow. Steady state CFD simulations were conducted using CFX v11.0.

### VELOCITY FIELD RESULTS

The blowing ratio is defined as  $BR = V_{jet} / V_{main}$ , where  $V_{jet}$  is the bulk averaged slot jet velocity and  $V_{main}$  is the bulk averaged mainstream velocity at  $x_s$ . All results presented in this paper are for  $BR = 1.3$  and  $Re = 110,000$  where  $Re$  is based on  $V_{main}$  and the airfoil chord length. Velocity profiles from the CFD results and the MRV measurements at three locations downstream of the slots are compared for the spanwise center ( $z = 0$  mm) of the airfoil in Figure 5. The regions with zero velocities identify solid airfoil material. Good agreement between the computation and experiment is seen especially along the surface of the breakout. At  $x/h = 50$ , which is 2 slot heights or 25% of the breakout length downstream of the slot exit, the streamwise jet velocities are nearly identical, with deviations in both components on the suction (negative in  $y$ ) and pressure (positive in  $y$ ) sides of the airfoil. After the trailing edge ( $x/h = 56.6$ ) differences are more pronounced with evidence of more rapid mixing in the streamwise component for the MRV data. Wall normal velocities in this region still compare well.

Figure 5 shows that in the region immediately behind the slots, the simulation and experiment agree within the uncertainty of the measurements. In the wake, the simulation and the experiments show a larger difference, indicating that the turbulent shear layer introduces additional modeling challenges in this region.

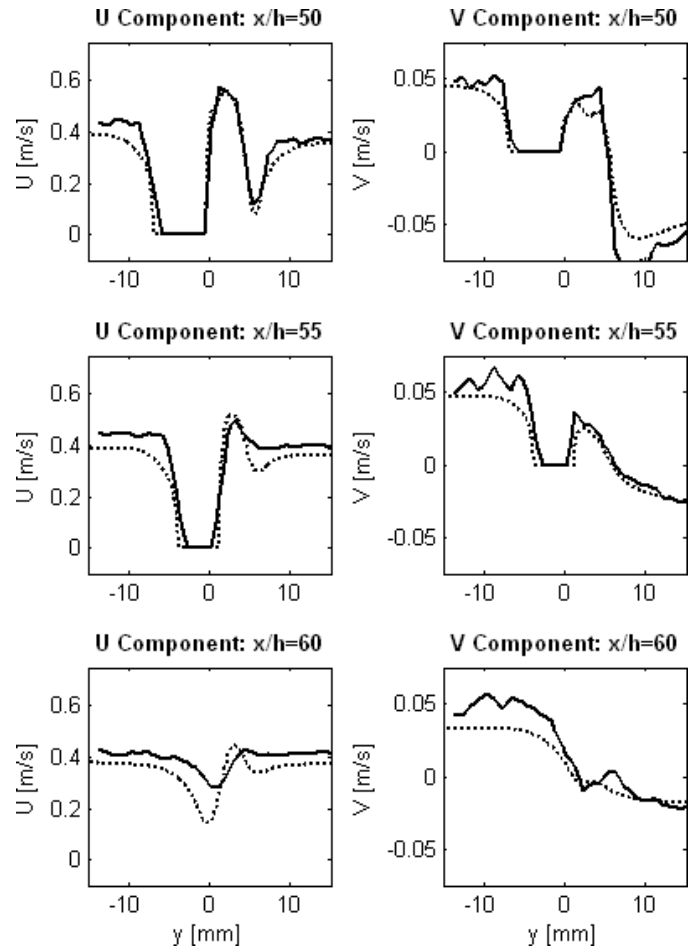
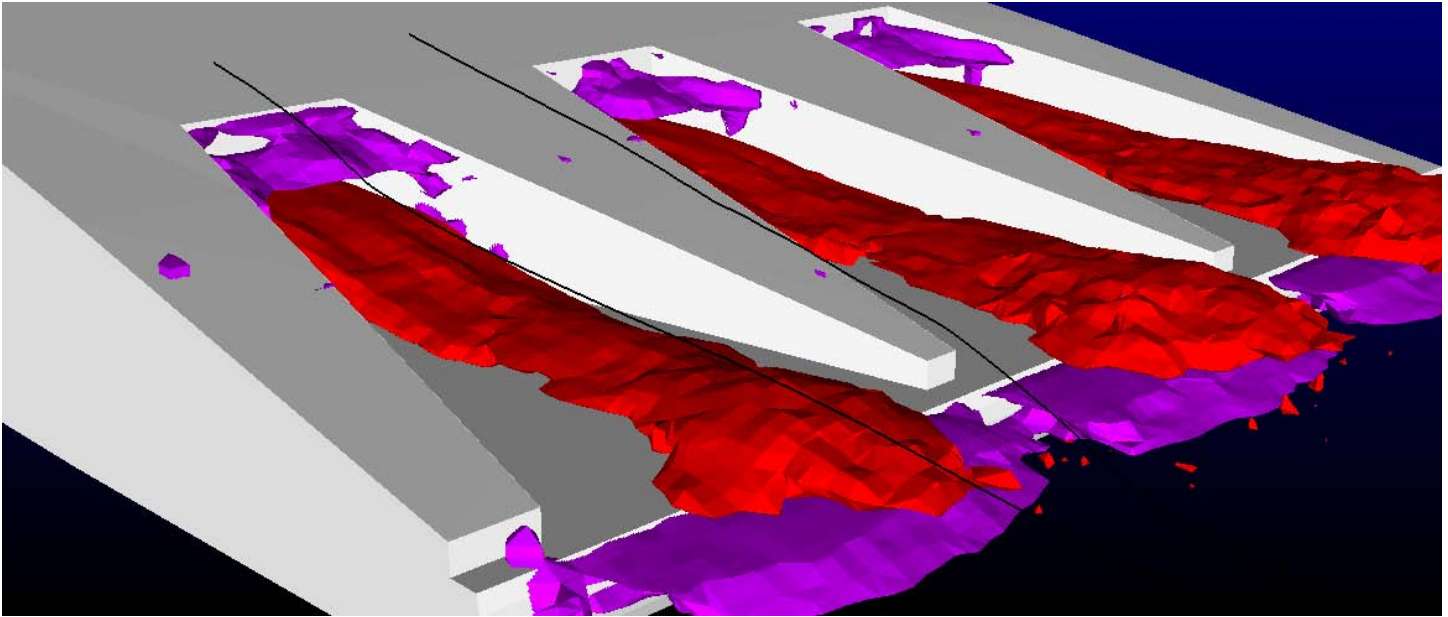


Figure 5 – Velocity profiles for CFD (dashed) and MRV (solid) at 3 streamwise locations



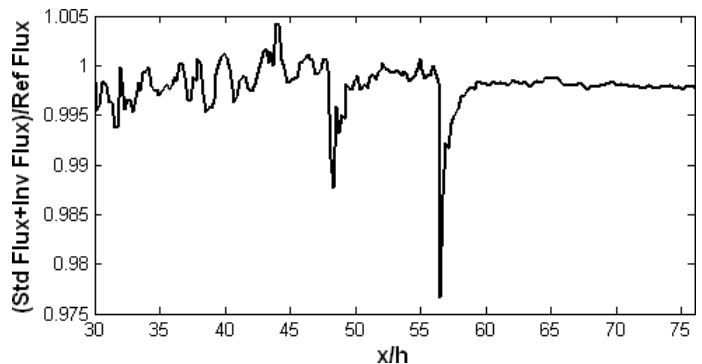
**Figure 6 – Iso-surfaces of fast (red) and reverse (purple) flow for the trailing edge.  $U \geq 1.3 \cdot U_{\text{main}}$  are shown in red. Streamlines in black depict freestream flow from positions centered above the slot and land**

Figure 6 is a perspective view of the trailing edge region in which the purple color marks a zero streamwise mean velocity iso-surface. The airfoil surface is indicated in white. Slight differences are evident between individual slot flow rates and velocities. The red iso-surfaces indicate where mean streamwise velocity is 30% higher than the mainstream velocity at the slot exit which matches the unmixed coolant jet velocity since  $BR=1.3$ . This view reveals separation bubbles behind the slot lip and behind the blunt trailing edge of the airfoil. Both of these separation bubbles are very short. For example, the bubble behind the slot lip closes after 1.2 slot heights. This means that the streamlines passing over the center of the slot curve sharply downward as compared to a streamline above the center of a land which has only mild curvature. Therefore, a strong spanwise pressure gradient must exist in that region, which strengthens mean secondary flows. Three-dimensional distortions of separated shear layers are known to enhance turbulent mixing. The CFD results show significantly longer separation bubbles, which could reduce the strength of computed secondary flows. Additionally, the lack of significant separation in the wake of the lands is due to strong wall normal velocities towards the suction side of the airfoil, as near land vortices from each side of the lands interact. Streaks of coolant flow entrained in these vortices emerge coherently downstream on the airfoil suction side.

### CONCENTRATION FIELD RESULTS

To date, the CFD work only includes the velocity field. All concentration and velocity field data presented below are from experimental measurements. The uncertainty in the MRC measurements is estimated at 6.0% near surfaces and 5.1% in the wake region. This estimate combines three contributions in

a root sum squares technique. First, the statistical uncertainty of the point by point concentration calculations, based on the variability of the data and the total number of runs by type conducted is calculated for the entire flow field. The flowmeter uncertainty is also included. A final contribution is due to corrections made to account for non-uniform sensitivity in the x-direction, accounted for in Equation 1. The adequacy of these corrections is tested by evaluation of the concentration flux at each streamwise position. Ideally, the same exact concentration flux would be measured at every streamwise position. The sum of the concentration flux obtained in the standard and inverted runs was divided by the reference case flux across all y and z elements at each streamwise location. Maximum deviations from the nominal value of 1.0 at each position are the final contribution to uncertainty, and are generally small, as indicated in Figure 7.



**Figure 7 – Concentration flux at each streamwise position.**

The concentration field that emerges from the slots evolves downstream in a non-uniform manner. Figure 8 shows a 10% concentration iso-surface for the trailing edge region. This figure essentially shows the outer boundary of the coolant field. The coolant jet broadens as the lands diverge and forms symmetric troughs inboard of the lands. Also, coolant is entrained into the separation bubble behind the slot lip. It is important to note that the coolant does not reach the top of the land surfaces, though it does extend above the land height at the sides of the lands.

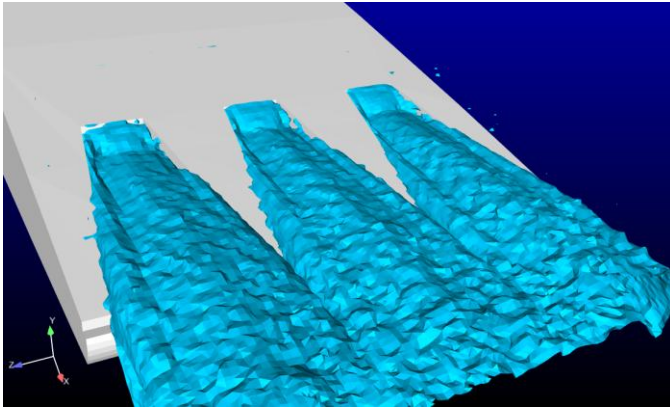


**Figure 8 – The 10% concentration iso-surface**

The most widely studied parameter for film cooled turbine blades is the surface effectiveness defined in Equation 5.

$$\eta_{AW} = \frac{T_H - T_{AW}}{T_H - T_C} = \frac{C_H - C_{AW}}{C_H - C_C} = C_{AW} \quad (5)$$

In Equation 5, the subscripts H and C refer to the mainstream (H) and coolant (C) flows, while AW stands for the adiabatic wall temperature recorded in a thermal experiment. The analogous concentration equation, given appropriate assumptions for fluid properties is included in Equation 5. Direct measurement of this quantity requires an adiabatic boundary condition on the test surface. Adiabatic conditions are difficult to achieve in experiments, so thermal measurements of effectiveness often require detailed corrections [11, 13, 18]. An alternative is a concentration based measurement where the analogous boundary condition of zero mass flux through the surface is easily obtained. As seen in Equation 5, the wall concentration is the surface effectiveness.

Figure 9 shows the film cooling surface effectiveness using the concentration measurement closest to the surface at each point. There is an extended core region covering over 60% of the trailing edge, using a definition of core suggested in [6] as the region where the spanwise average is above 90%. The surface effectiveness very near the lands between 1 and 4 slot heights downstream of the slot is low which may in part be due to the slot lip separated region which extends down along the

land walls in this region, see Figure 6. However, the 1 mm resolution of the measurements in the spanwise and streamwise directions should be considered when observing the smallest regions with low effectiveness. With these small exceptions, the distribution of coolant across the surface generally varies by less than 15%. This is important for the blade designer who can use the distribution to calculate the effects of thermal stresses on the lifetime of the blade.

The spanwise averaged film cooling effectiveness (Figure 10) is a parameter that also receives attention in trailing edge cooling studies. It is calculated by averaging the surface effectiveness across only the breakout floor at each streamwise position. A high concentration core region ends after a distance of 5 slot heights downstream, and is followed by a rapid decay of the surface effectiveness.

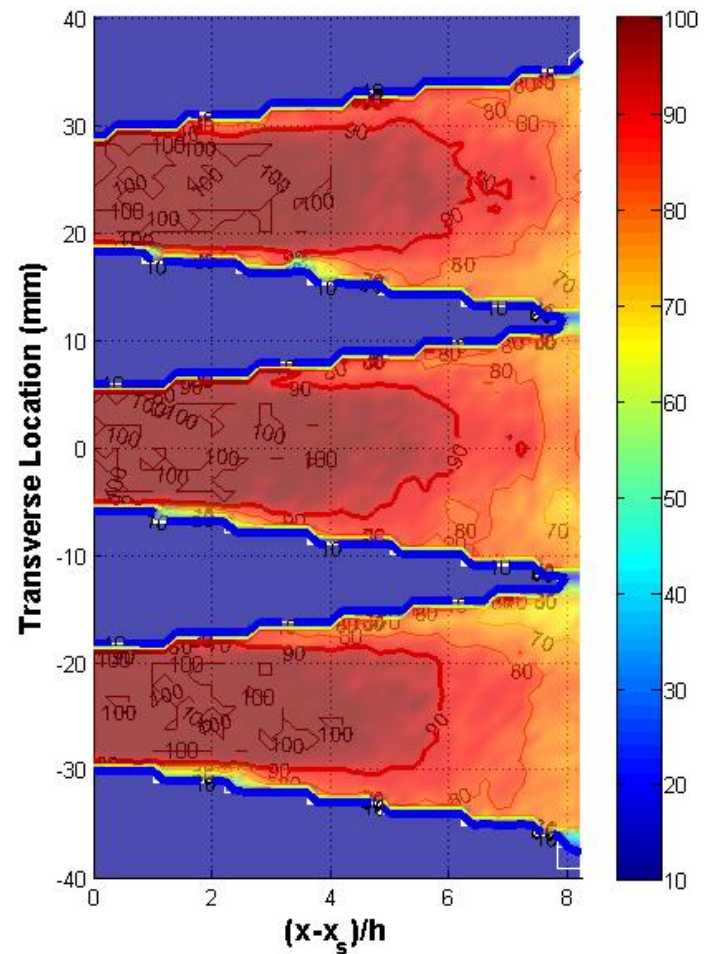


**Figure 9 - Surface effectiveness for the three slots. 90% Effectiveness Contour Highlighted**

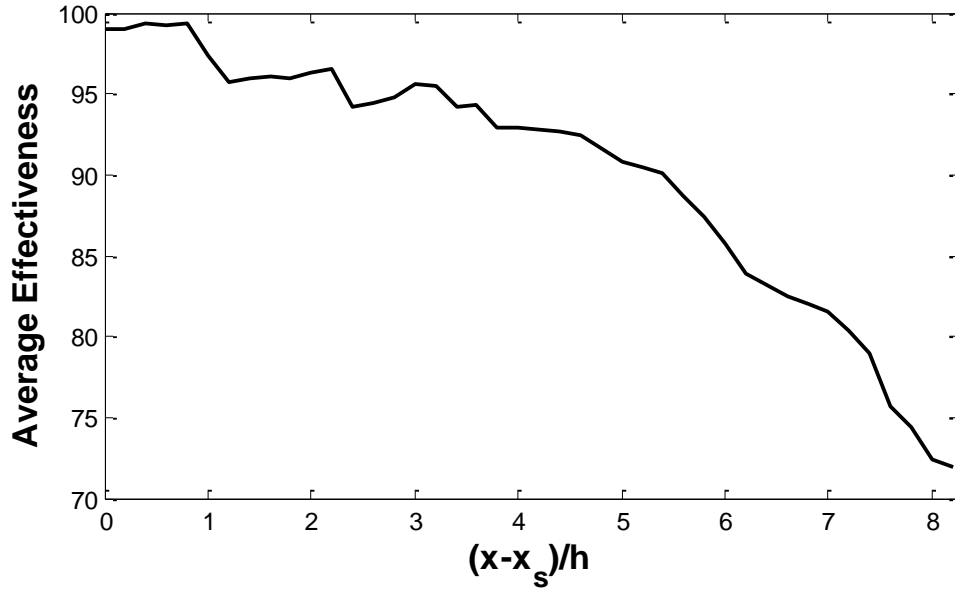


Figure 10 – Spanwise averaged surface effectiveness variation downstream of slot exit

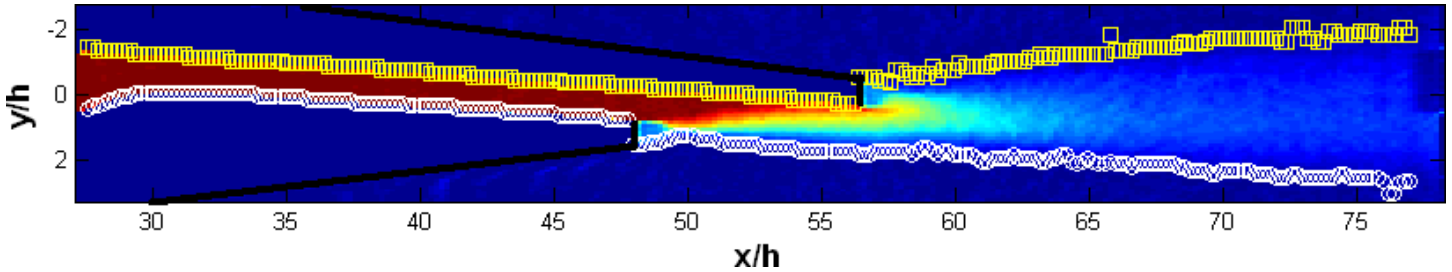


Figure 11 – Wake dispersion from the middle of the center slot jet. Lines added to highlight airfoil exterior edges

Wake mixing and dispersion represents one region of the coolant field where little attention has been given in recent experimental work. Trailing edge wake pressure and velocity fields have been studied for evidence of unsteady behavior and their impact on downstream vanes and blades [5, 16, 17]. However, the dispersion of the trailing edge coolant has not received much experimental attention, so engineers rely primarily on turbulent shear layer and wall jet studies to predict downstream effects. Figure 11 depicts the mixing layer development in the centerplane of the middle slot jet. The edges of the coolant field are identified with colored squares to assist in identifying the spreading angle of the jet, which in this particular case has an average spreading angle in the wake region of  $6.0^\circ$ . The suction side of the airfoil is the top half of the figure.

The concentration field in the wake allows for the analysis of coolant streaks that may impact design consideration for downstream vanes and turbine blade stages. Figure 12 shows the concentration distribution in a spanwise-vertical ( $z$ - $y$ ) plane downstream of the trailing edge.

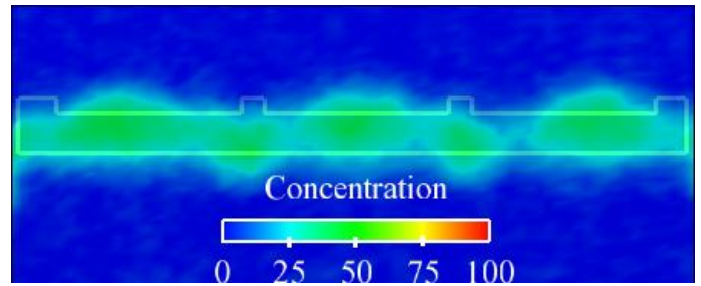


Figure 12 – Measured coolant field 4 slot heights downstream of the trailing edge

The plane has been made partially transparent to show the relation to the key features of the trailing edge upstream. There are five streaks emerging from the three slots and two land tips away from the channel walls of the test section. The land tip streaks move toward the suction side of the airfoil, while the slot center streaks stay on the pressure side. These streaks are still present 4 slot heights downstream of the trailing edge with coolant concentrations at 50%. This means that the temperature distribution impinging on downstream components may be very

non-uniform, a potentially important feature to capture in simulation or design. Evidence of these streaks persists through the image domain as is also indicated in Figure 11.

### COMBINED FIELD ANALYSIS

Together, the surface effectiveness and spanwise averaged effectiveness are the primary tools utilized in analysis of turbine blade trailing edges. However, they represent only a portion of the information that can be leveraged from the full data set of the velocity and concentration fields. For example, the shape of the coolant field can provide insight into regions where there might be too much or too little coolant, information critical to effective design. Figure 13 shows contours representing the concentration field with in plane velocity vectors for the spanwise centerplane of the middle slot. Several features are immediately apparent. First, the separation bubble, evident from the low concentration region near the upper left edge of the figure, prevents mainstream fluid from any substantive mixing. After the bubble closes, however, the mainstream flow follows the curvature and accelerates into the coolant at a high angle. The strong streamline curvature associated with the rapid closure of the separation bubble is a source of strong secondary flows and probably aggressive mixing at the edge of the coolant jet. There is no clear evidence of the impact of this streamline curvature at the surface in this region. Only through static pressure measurements or select computational analyses have other studies suggested the presence of this feature, such as in [2-3, 6, 19-20]. Secondly, following this region, a

turbulent shear layer grows but the coolant remains relatively unmixed at the surface. The end of this region, identified earlier as the extended core region, shows evidence of more rapid mixing, and the velocity vectors near the breakout surface indicate a turning of the coolant flow away from the surface in the wall normal direction, and into the mainstream fluid.

Figure 14 shows a second combined concentration and velocity field view. In this figure, five equally spaced streamwise planes of concentration contours are overlaid with the secondary velocity vectors. The planes are spanwise truncated to improve visibility. In addition, the surface and pressure side of the airfoil are visible as white/gray regions in this cross sectional view. The vectors clearly indicate that fluid from the tops of the land partitions sweep into a region just away from the land sidewall and mix into the coolant flow. This is perhaps most strongly evident in the fourth plane which is 7.2 slot heights downstream of the slot exit. The size of the rotational mixing structure is several millimeters in diameter, creating a region of low concentration near the surface.

The impact on the mixing by this longitudinal vortex results in an uneven coolant distribution near the trailing edge. The coolant field forms a three-pointed crown shown in Figure 15 which depicts a cross stream plane of concentration eight slot-heights or 93% of trailing edge length downstream of the slot exit. The uneven coolant distribution at the top of the coolant layer and at the surface implies that a design that more evenly distributes the coolant has a good chance of increasing the average film cooling effectiveness at the surface.

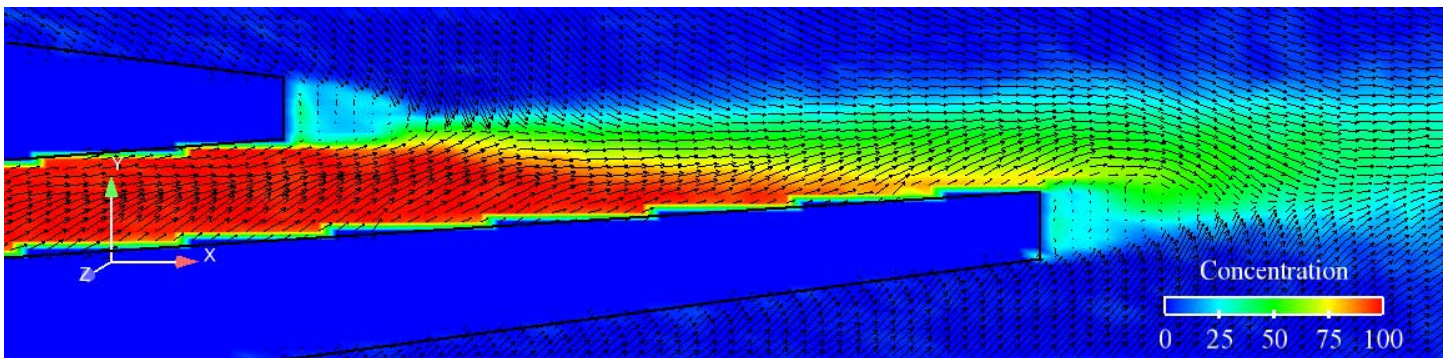


Figure 13 – Experimental concentration contours and velocity vectors for a slot centerplane. Lines added to emphasize airfoil surfaces

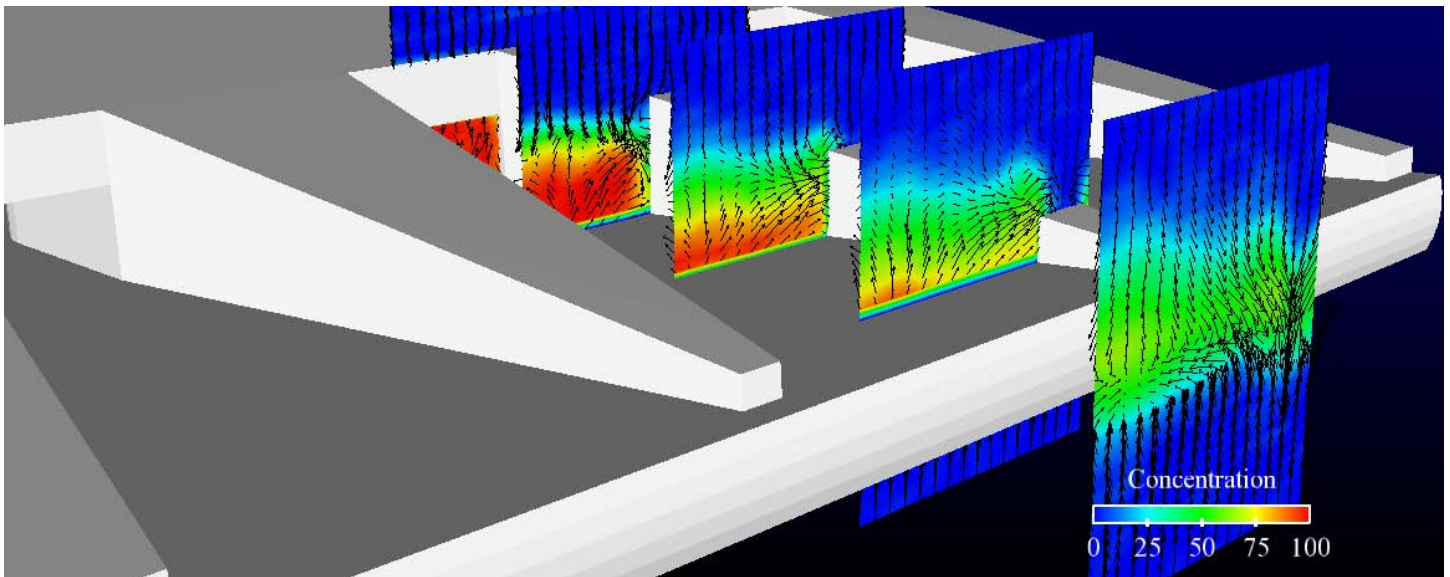


Figure 14 – Multiple planes of concentration contours with tangential velocity vectors

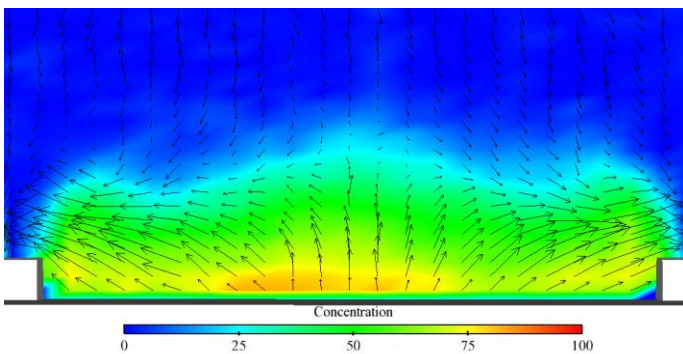


Figure 15 – Coolant distribution at 8 slot heights downstream of slot exit

## CONCLUSIONS

A new MRI-based diagnostic capable of quantifying 3D scalar and velocity fields is applied to a pressure side cutback trailing edge film cooling scheme. The combined concentration and velocity measurements allow insight into mechanisms contributing to the rapid mixing characteristic of trailing edge breakout flows. The velocity is compared to an unsteady RANS simulation with good agreement in several locations along the trailing edge breakout and in the wake region behind the trailing edge. A separation bubble behind the slot lip forms a region where little mixing can occur between the high temperature mainstream and coolant flows. However, very energetic turbulent mixing layers develop around the slot-lip separation bubble. These rapidly mix jet and mainstream fluid once the bubble closes. The three-dimensional geometry and the resulting vortex structures apparently enhance the turbulent mixing rate in this region. Once the shear layer spreads to the breakout surface, the surface effectiveness rapidly degrades. Surface effectiveness measurements with an uncertainty at 6.0%

show the regional impact of this mixing, with lower effectiveness values in regions near the land walls and across the breakout surface close to the trailing edge. The 3D concentration field coupled with velocity vectors highlights the longitudinal vortices from the lands scooping coolant fluid towards the lands, leaving troughs with low coolant concentration.

## ACKNOWLEDGMENTS

This work was funded both by the United States Army Research Office and the General Electric University Strategic Alliance program. The authors would like to thank Mr. Cory Williams at GEAE for providing support for this work. Use of the facilities at the Richard M. Lucas Center for Magnetic Resonance Spectroscopy and Imaging is gratefully acknowledged along with funded scan time from the Stanford Department of Radiology. The views expressed herein are those of the authors and do not purport to reflect the position of the Department of the Army, or the Department of Defense.

## NOMENCLATURE

BR	Blowing Ratio
Re	Reynolds Number
S	Standard Concentration Scan
I	Inverted Concentration Scan
R	Reference Concentration Scan
B	Background Concentration Scan
SF	Scale Factor
$\eta$	Adiabatic Film Cooling Effectiveness
H	High Temperature Mainstream Fluid
C	Coolant Fluid
AW	Adiabatic Wall
MRI	Magnetic Resonance Imaging

MRC Magnetic Resonance Concentration measurement  
 MRV Magnetic Resonance Velocimetry  
 h Slot Height  
 $x_s$  Streamwise position of slot exit  
 Re Reynolds number

## REFERENCES

- [1] Holloway DS, Leylek JH, Buck FA, 2002, Pressure-Side Bleed Film Cooling: Part 2, Unsteady Framework for Experimental and Computational Results, ASME Paper No. GT2002-30472
- [2] Martini, P, Schulz, A, Bauer, H, Whitney, C, Detached Eddy Simulation of Film Cooling Performance on the Trailing Edge Cutback of Gas Turbine Airfoils, J Turbomach Vol 128, Apr 2006, pp 292-299
- [3] Joo, J, Durbin P, Simulation of Turbine Blade Trailing Edge Cooling, J Fluids Eng Vol 131, Feb 2009, pp 1-14
- [4] Taslim, M, Spring, S, Mehlman, B, Experimental Investigation of Film Cooling Effectiveness for Slots of Various Exit Geometries, J Thermophys Heat Tran Vol 6, No 2, Apr-Jun 1992, pp 302-307
- [5] Holloway DS, Leylek JH, Buck FA, 2002, Pressure-Side Bleed Film Cooling Part 1: Steady Framework for Experimental and Computational Results, ASME Paper No GT2002-30471
- [6] Martini, P, Schulz, A, Bauer, H, Film Cooling Effectiveness and Heat Transfer on the Trailing Edge Cutback of Gas Turbine Airfoils with Various Internal Cooling Designs. J Turbomach Vol 128, Jan 2006, pp 196-205
- [7] Cunha, F, Chyu, M, Trailing-Edge Cooling for Gas Turbines. J Prop Power Vol 22, No 2, Mar-Apr 2006, pp 286-300
- [8] Choi, J, Mhetras, S, Lau, S, Rudolph, R, Film Cooling and Heat Transfer on Two Cutback Trailing Edge Models with Internal Perforated Blockages. J Heat Tran Vol 130, Jan 2008, pp 1-13
- [9] Dannhauer, A, 2009, Investigation of Trailing Edge Cooling Concepts in a High Pressure Turbine Cascade – Analysis of the Adiabatic Film Cooling Effectiveness, ASME Paper No GT2009-59343
- [10] Krueckels, J, Gritsch, M, Schnieder, M, 2009, Design Considerations and Validation of Trailing Edge Pressure Side Bleed Cooling, ASME Paper No GT2009-59161
- [11] Fiala, N, Jaswal, I, Ames, F, Letterbox Trailing Edge Heat Transfer: Effects of Blowing Rate, Reynolds Number, and External Turbulence on Heat Transfer and Film Cooling Effectiveness, J. Turbomach Vol 132, Jan 2010, pp 1-10
- [12] Elkins, C, Alley, M, Magnetic Resonance Velocimetry: Applications of Magnetic Resonance Imaging in the Measurement of Fluid Motion, Exp Fluids Vol 43, 2007, pp 823-858
- [13] Benson, M, Measurements of 3D Velocity and Scalar Field for a Film-Cooled Airfoil Trailing Edge, Stanford University Dissertation, 2011
- [14] Benson, M, Elkins, C, Mobley, P, Alley, M, Eaton J, Three Dimensional Concentration Field Measurements in a Mixing Layer Using Magnetic Resonance Imaging, Exp Fluids 2010, Vol 49, No 1, pp 43-55
- [15] Elkins CJ, Markl M, Pelc N., Eaton, 4D Magnetic Resonance Velocimetry for Mean Velocity Measurements in Complex Turbulent Flows, Exp Fluids 2003, Vol 34, No 4, pp 494-503
- [16] Chen, Y, Matalanis, C, Eaton, J, High Resolution PIV Measurements Around a Model Turbine Blade Trailing Edge Film-Cooling Breakout, Exp Fluids 2008, Vol 44, pp 199-209
- [17] Laskowski, G, Felten, F, Steady and Unsteady CFD Simulations of Transonic Turbine Vane Wakes with Trailing Edge Cooling, European Conference on Computational Fluid Dynamics, June 2010
- [18] Baldauf, S, Scheurlen, M, Correlation of Film-Cooling Effectiveness from Thermographic Measurements at Engine-like Conditions, J Turbomach Vol 124, Oct 2002, pp 686-698
- [19] Burns, W, Stollery, J, The Influence of Foreign Gas Injection and Slot Geometry on Film Cooling Effectiveness Int J Heat Mass Transfer Vol 12, 1968, pp935-951
- [20] Bittlinger, G, Schulz, A, Wittig, S, 1994, Film Cooling Effectiveness and Heat Transfer Coefficients for Slot Injection at High Blowing Ratios, ASME Paper No GT1994-182